Influence of birefringence in the instability spectra of oppositely directed coupler with negative index material channel

A. K. Shafeeque Ali,[1] K. Nithyanandan,[1] K. Porsezian,[1,*] and Andrei I. Maimistov[2]

[1]*Department of Physics, Pondicherry University, Pondicherry 605014, India*

[2]*Department of Solid State Physics and Nanostructures, National Research Nuclear University MEPhI, Kashirskoe sh. 31, Moscow, 115409, Russian Federation*

(Received 26 November 2015; published 29 February 2016)

A theoretical investigation on the influence of birefringence in the modulational instability (MI) spectra of an oppositely directed coupler (ODC) with a negative index material (NIM) channel is presented. We study the effect of birefringence on MI in linear and circular birefringent ODCs for both normal and anomalous dispersion regimes. It is found that besides the instability band due to nonlinear positive index material (PIM) and negative index material (NIM) channels, new symmetric instability regions are observed as a result of birefringent effects. Also defocusing nonlinearity suppresses the NIM band in the normal dispersion regime, but in the anomalous dispersion regime the defocusing nonlinearity enhances the gain of the NIM band. In contrast to the case of linear birefringence, in terms of MI gain from circular birefringence, only two birefringent bands dominate: the inherently PIM and NIM bands. This preponderance is attributed to the fact that the cross-phase modulation effect for the case of circular birefringence is stronger, thus allowing a better coupling between the beams, which results in the enhancement of the gain. Therefore, the manipulation of MI and solitons in an ODC is better performed when the birefringence is circular rather than linear. Here we report how to generate and manipulate MI and solitons in birefringent ODCs with a particular emphasis on a NIM channel.

DOI: 10.1103/PhysRevA.93.023848

I. INTRODUCTION

Modulation instability (MI) is a fundamental and ubiquitous process that appears in most nonlinear systems [1–4]. During this process, small perturbations upon a uniform intensity beam grow exponentially due to the interplay between nonlinearity and dispersion or diffraction. As a result, a continuous wave often breaks up into trains of ultrashort solitons like pulses [5]. MI is closely related to the Fermi-Pasta-Ulam recurrence effect and to the existence of both bright and dark solitons. MI was first theoretically predicted by Hasegawa [6] in 1984 and later experimentally verified by Tai *et al.* in 1986 [7]. This nonlinear instability process has been observed in a large variety of subfields of physics, such as fluid dynamics [8], plasma [9–11], Bose-Einstein condensates [12,13], and nonlinear optics [14–17].

Recently, the propagation of electromagnetic waves through an oppositely directed coupler (ODC) with a negative index material (NIM) channel has attracted wide spread interest [18–20]. This coupler preserves the path of light propagation, but the direction of input and output fields are exactly opposite in nature, hence it is called an oppositely directed coupler [18]. The electromagnetic wave entering in one channel of the coupler leaves through the other channel in the opposite direction, which closely resembles a distributed mirror [21]. The NIM channel possesses an effective feedback mechanism due to the opposite directionality of the phase velocity and the energy flow. Through this effective feedback mechanism, the ODC admits gap soliton formation and possesses bistable properties [18].

The MI formulation in the context of an ODC, is connected with the coupled nonlinear Schrödinger equation (NLSE), which describes the propagation of electromagnetic waves in a couplerlike system. Depending on the power of the intense beam, by incorporating the various physical effects, the NLSE can be extended to study various physical phenomena. Recently, there has been growing interest in the study of MI in ODCs [20,22–26]. A crucial factor in the dynamics of MI in an ODC is the ratio of forward- to backward-propagating wave power. In Ref. [22], the author reported the impact of the forward- to backward-propagating power ratio and observed threshold conditions for the existence of MI in ODCs. MI in ODCs in the context of saturable nonlinear response and quintic nonlinearity was discussed in Refs. [23] and [24], respectively. It has been reported that both saturable nonlinearity and quintic nonlinearity significantly effect the MI spectrum and can be used to control the generation of MI bands. The effects of self-steepening (SS) and intrapulse Raman scattering (IRS) were studied in Ref. [20], and it has been found that SS and IRS generate new instability bands and extend the domain of the instability region.

All previous studies of MI in an ODC [20,22–24] ignored the birefringence effect caused by copropagation of the two polarized modes. The real single-mode fibers are not truly single modal but rather bimodal due to the presence of birefringence. The coupler structure considered in this paper is shown schematically in Fig. 1. There are a good number of studies devoted to the study of various nonlinear effects associated with the birefringent fibers. For instance, the dynamics of dark solitons in birefringent fibers was discussed by Akhmediev *et al.* [27], the polarization dynamics of birefringent fibers was reported in Ref. [28], and the generation of ultrashort pulses using birefringent fibers was discussed in Ref. [29], to mention a few. The study of MI in birefringent fibers deserves special attention, as it results in the generation of unconventional MI bands [30–33]. A comprehensive study of MI with the effect of stimulated Raman scattering in

*ponzsol@yahoo.com

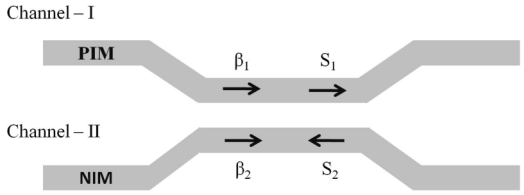

FIG. 1. Schematic diagram of a two core oppositely directed coupler.

birefringent fibers was reported by Millot *et al.* [30]. The enhancement of transmission capacity of an optical fiber as a result orthogonal polarizations was described in Ref. [34]. Recently, many interesting results have been reported in the context of polarization or vector MI [35–37]. For instance, polarization MI in a Manakov fiber system was discussed in Ref. [35]. In Refs. [36,37], Baronio *et al.* demonstrated the origin of rogue waves from baseband MI. Thus, considering the physical importance of birefringence, we derive a nonlinear propagation model for birefringent ODCs and investigate the effect of birefringence on the instability spectra of an ODC with a NIM channel.

The paper is organized as follows. In Sec. II, the theoretical model of the problem and linear stability analysis leading to the dispersion relation are presented. In Sec. III investigations of MI in a birefringent ODC with a NIM channel are carried out in detail, followed by conclusions in Sec. IV.

II. THEORETICAL MODEL

Let us consider the single-mode waveguides, whose electric field $\vec{E}(\omega)$ can be represented as [38,39]

$$E_x = \mathcal{E}_x^{(1)}(z,t)F_1^{(x)}(x,y)e^{i(\beta_{1x}z-\omega_0 t)} + \mathcal{E}_x^{(2)}(z,t) \times F_2^{(x)}(x,y)e^{i(\beta_{2x}z-\omega_0 t)} + \text{c.c.}, \tag{1a}$$

$$E_y = \mathcal{E}_y^{(1)}(z,t)F_1^{(y)}(x,y)e^{i(\beta_{1y}z-\omega_0 t)} + \mathcal{E}_y^{(2)}(z,t) \times F_2^{(y)}(x,y)e^{i(\beta_{2y}z-\omega_0 t)} + \text{c.c.}, \tag{1b}$$

where β_{ax} and β_{ay} are the propagation constants for the ath ($a = 1,2$) waveguide. Radial distribution of the electric field in the waveguide is defined by the mode functions $F_1^{(x)}(x,y)$ and $F_2^{(x)}(x,y)$ for the x component of the electrical field, and $F_1^{(y)}(x,y)$ and $F_2^{(y)}(x,y)$ for the y component.

The wave equation can be written as

$$\nabla^2\vec{E}(\omega) + k_0^2\hat{\varepsilon}(\omega,x,y)\cdot\vec{E}(\omega) = 0. \tag{2}$$

Here, $k_0 = \omega_0/c$ is the wave number of the carrier wave in a vacuum. If the waveguides are manufactured from metamaterials, then the equation can be modified as

$$\nabla^2\vec{E}(\omega) + k_0^2\hat{\varepsilon}(\omega,x,y)\hat{\mu}(\omega,x,y)\cdot\vec{E}(\omega) = 0. \tag{3}$$

Now we take the strong ansatz, the dielectric tensor $\hat{\varepsilon}$ is a diagonal one $\hat{\varepsilon} = \text{diag}(\varepsilon_x,\varepsilon_y,\varepsilon_z)$. Thus the wave equation splits into two scalar equations

$$\nabla^2 E_x(\omega) + k_0^2\varepsilon_x(\omega,x,y)E_x(\omega) = 0,$$

$$\nabla^2 E_y(\omega) + k_0^2\varepsilon_y(\omega,x,y)E_y(\omega) = 0.$$

Operator ∇^2 is $\partial^2/\partial z^2 + \nabla_\perp^2$. By using the slowly varying approximation, we can write

$$\left(2i\beta_{1x}\frac{\partial\mathcal{E}_x^{(1)}}{\partial z} - \beta_{1x}^2\mathcal{E}_x^{(1)}\right)e^{i\beta_{1x}z}F_1^{(x)} + \left(2i\beta_{2x}\frac{\partial\mathcal{E}_x^{(2)}}{\partial z} - \beta_{2x}^2\mathcal{E}_x^{(2)}\right)e^{i\beta_{2x}z}F_2^{(x)} + \mathcal{E}_x^{(1)}e^{i\beta_{1x}z}\nabla_\perp^2F_1^{(x)} + \mathcal{E}_x^{(2)}e^{i\beta_{2x}z}\nabla_\perp^2F_2^{(x)} + k_0^2\varepsilon_x\left(\mathcal{E}_x^{(1)}e^{i\beta_{1x}z}F_1^{(x)} + \mathcal{E}_x^{(2)}e^{i\beta_{2x}z}F_2^{(x)}\right) = 0. \tag{4a}$$

$$\left(2i\beta_{1y}\frac{\partial\mathcal{E}_y^{(1)}}{\partial z} - \beta_{1xy}^2\mathcal{E}_y^{(1)}\right)e^{i\beta_{1y}z}F_1^{(y)} + \left(2i\beta_{2y}\frac{\partial\mathcal{E}_y^{(2)}}{\partial z} - \beta_{2y}^2\mathcal{E}_y^{(2)}\right)e^{i\beta_{2y}z}F_2^{(y)} + \mathcal{E}_y^{(1)}e^{i\beta_{1y}z}\nabla_\perp^2F_1^{(y)} + \mathcal{E}_y^{(2)}e^{i\beta_{2y}z}\nabla_\perp^2F_2^{(y)} + k_0^2\varepsilon_y\left(\mathcal{E}_y^{(1)}e^{i\beta_{1y}z}F_1^{(y)} + \mathcal{E}_y^{(2)}e^{i\beta_{2y}z}F_2^{(y)}\right) = 0. \tag{4b}$$

The mode functions $F_1^{(x)}$, $F_2^{(x)}$, $F_1^{(y)}$, and $F_2^{(y)}$ are defined by

$$\nabla_\perp^2F_a^{(\alpha)} + \left(k_0^2\varepsilon_\alpha^{(a)} - \beta_{a\alpha}^2\right)F_a^{(\alpha)} = 0, \tag{5}$$

where $a = 1,2$ and $\alpha = x,y$. Using these equations one can modify the wave equations. The equation for the electric field in the first waveguide E_x leads to

$$2i\beta_{1x}\frac{\partial\mathcal{E}_x^{(1)}}{\partial z}e^{i\beta_{1x}z}F_1^{(x)} + 2i\beta_{2x}\frac{\partial\mathcal{E}_x^{(2)}}{\partial z}e^{i\beta_{2x}z}F_2^{(x)} + k_0^2\left(\varepsilon_x - \varepsilon_x^{(1)}\right) \times \mathcal{E}_x^{(1)}e^{i\beta_{1x}z}F_1^{(x)} + k_0^2\left(\varepsilon_x - \varepsilon_x^{(2)}\right)\mathcal{E}_x^{(2)}e^{i\beta_{1x}z}F_2^{(x)} = 0.$$

The functions $F_1^{(x)}$ and $F_1^{(y)}$ are localized in the first waveguide, and the functions $F_2^{(x)}$ and $F_2^{(y)}$ are localized in the second waveguide. Thus, we can assume the following approximation:

$$\langle F_1,\alpha|F_2,\beta\rangle = \int F_1^{(\alpha)}(x,y)F_2^{(\beta)}(x,y)dx\,dy = 0.$$

Let

$$\langle F_a,\alpha|F_a,\alpha\rangle = \int F_a^{(\alpha)}(x,y)F_a^{(\alpha)}(x,y)dx\,dy = 1.$$

These assumptions allow us to get two equations:

$$2i\beta_{1x}\frac{\partial\mathcal{E}_x^{(1)}}{\partial z} + k_0^2\langle F_1,x|\left(\varepsilon_x - \varepsilon_x^{(1)}\right)|F_1,x\rangle\mathcal{E}_x^{(1)} + k_0^2\langle F_1,x|\left(\varepsilon_x - \varepsilon_x^{(2)}\right)|F_2,x\rangle\mathcal{E}_x^{(2)}e^{iz(\beta_{2x}-\beta_{1x})} = 0, \tag{6a}$$

$$2i\beta_{2x}\frac{\partial \mathcal{E}_x^{(2)}}{\partial z} + k_0^2\langle F_2,x|\left(\varepsilon_x - \varepsilon_x^{(2)}\right)|F_2,x\rangle\mathcal{E}_x^{(2)} + k_0^2\langle F_2,x|\left(\varepsilon_x - \varepsilon_x^{(1)}\right)|F_1,x\rangle\mathcal{E}_x^{(1)}e^{-iz(\beta_{2x}-\beta_{1x})} = 0. \quad (6b)$$

In the integral $\langle F_1,x|(\varepsilon_x - \varepsilon_x^{(1)})|F_1,x\rangle$ the difference $\varepsilon_x - \varepsilon_x^{(1)}$ is localized in the region of the second waveguide, but $F_1^{(x)2}$ is localized in the region of first waveguide. Thus this integral approximately is zero. Under the near-zero mismatch conditions, the coupling constants can be defined as

$$\kappa^\alpha = \frac{k_0^2\langle F_2,\alpha|\left(\varepsilon_\alpha - \varepsilon_\alpha^{(2)}\right)|F_1,\alpha\rangle}{2\beta_{1\alpha}} \approx \frac{k_0^2\langle F_1,\alpha|\left(\varepsilon_\alpha - \varepsilon_\alpha^{(1)}\right)|F_2,\alpha\rangle}{2\beta_{2\alpha}}.$$

Finally, the equations for $\mathcal{E}_\alpha^{(a)}$ take the form

$$i\frac{\partial \mathcal{E}_\alpha^{(1)}}{\partial z} + \kappa^\alpha \mathcal{E}_\alpha^{(2)}e^{iz(\beta_{2\alpha}-\beta_{1\alpha})} = 0, \quad (7a)$$

$$i\frac{\partial \mathcal{E}_\alpha^{(2)}}{\partial z} + \kappa^\alpha \mathcal{E}_\alpha^{(1)}e^{-iz(\beta_{2\alpha}-\beta_{1\alpha})} = 0. \quad (7b)$$

According to [38,39] we introduce the birefringence parameters

$$\beta_{ax} = \beta + \Delta\beta_a, \quad \beta_{ay} = \beta - \Delta\beta_a, \quad a = 1,2.$$

Hence,

$$\beta_{2x} - \beta_{1x} = \Delta\beta + \delta\beta, \quad \beta_{2y} - \beta_{1y} = \Delta\beta - \delta\beta,$$

where $\Delta\beta = \beta - \beta_1$ and $\delta\beta = \Delta\beta - \Delta\beta_1$.

It is suitable to introduce new envelopes A_x, A_y, B_x, and B_y:

$$\mathcal{E}_x^{(1)} = A_x e^{iz(\Delta\beta+\delta\beta)/2}, \quad \mathcal{E}_x^{(2)} = B_x e^{-iz(\Delta\beta+\delta\beta)/2},$$
$$\mathcal{E}_y^{(1)} = A_y e^{iz(\Delta\beta-\delta\beta)/2}, \quad \mathcal{E}_y^{(2)} = B_y e^{-iz(\Delta\beta-\delta\beta)/2}.$$

In terms of these envelopes the system of Eqs. (7a) and (7b) can be rewritten as

$$i\frac{\partial A_x}{\partial z} - \frac{\Delta\beta+\delta\beta}{2}A_x + \kappa^x B_x = 0, \quad (8a)$$

$$i\frac{\partial A_y}{\partial z} + \frac{\Delta\beta-\delta\beta}{2}A_y + \kappa^y B_y = 0, \quad (8b)$$

$$i\frac{\partial B_x}{\partial z} + \frac{\Delta\beta+\delta\beta}{2}B_x + \kappa^x A_x = 0, \quad (8c)$$

$$i\frac{\partial B_y}{\partial z} - \frac{\Delta\beta-\delta\beta}{2}B_y + \kappa^y A_y = 0. \quad (8d)$$

If we consider the electromagnetic pulse propagation in these equations the following substitution needs to be incorporated:

$$\frac{\partial}{\partial z} \to \sigma\frac{\partial}{\partial z} + \frac{1}{v_{a\alpha}}\frac{\partial}{\partial t}.$$

Here, $\sigma = \pm 1$. The substitution of the nonlinear polarization can be done by standard approach as follows. Then the propagation of the light wave in a birefringent ODC with a NIM channel can be described by the following four coupled nonlinear Schrödinger equations (CNLSEs):

$$i\sigma_1\frac{\partial A_x}{\partial z} + i\frac{1}{v_{1x}}\frac{\partial A_x}{\partial t} - \frac{\Delta\beta+\delta\beta}{2}A_x + k_{12x}B_x + \gamma_{1x}(|A_x|^2 + \rho|A_y|^2)A_x = 0, \quad (9a)$$

$$i\sigma_1\frac{\partial A_y}{\partial z} + i\frac{1}{v_{1y}}\frac{\partial A_y}{\partial t} + \frac{\Delta\beta-\delta\beta}{2}A_y + k_{12y}B_y + \gamma_{1y}(|A_y|^2 + \rho|A_x|^2)A_y = 0, \quad (9b)$$

$$i\sigma_2\frac{\partial B_x}{\partial z} + i\frac{1}{v_{2x}}\frac{\partial B_x}{\partial t} + \frac{\Delta\beta+\delta\beta}{2}B_x + k_{21x}A_x + \gamma_{2x}(|B_x|^2 + \rho|B_y|^2)B_x = 0, \quad (9c)$$

$$i\sigma_2\frac{\partial B_y}{\partial z} + i\frac{1}{v_{2y}}\frac{\partial B_y}{\partial t} - \frac{\Delta\beta-\delta\beta}{2}B_y + k_{21y}A_y + \gamma_{2y}(|B_y|^2 + \rho|B_x|^2)B_y = 0, \quad (9d)$$

where σ_1 and σ_2 indicate the sign of refractive index in channel one (C1) and channel two (C2), respectively. We consider that C1 is made of positive index material (PIM) and C2 by NIM, hence $\sigma_1 = 1$ and $\sigma_2 = -1$; A_j and B_j $(j = x,y)$ are the normalized complex amplitude of the modes in PIM and NIM channels, respectively; γ_{ij} and v_{ij} are the normalized nonlinear coefficients and absolute value of group velocities for C1 and C2, respectively. k_{12j} and k_{21j} are coupling coefficients, and ρ is the relative cross phase modulation coefficient. We assume the following forms of steady-state solutions for Eq. (9):

$$A_x = u_{1x}\exp(iq_1 z), \quad (10a)$$

$$A_y = u_{1y}\exp(iq_2 z), \quad (10b)$$

$$B_x = u_{2x}\exp(iq_1 z), \quad (10c)$$

$$B_y = u_{2y}\exp(iq_2 z), \quad (10d)$$

where q_i is the propagation constant corresponding to the different polarization components and u_{ij} is the constant amplitude. We use linear stability analysis to study MI in an ODC based on Eq. (9). The basic idea of linear stability analysis is to perturb a continuous-wave solution and then analyze whether the perturbation grows or decays with propagation. The linear stability of the steady state can be examined by perturbing the solutions of the following form:

$$a_{1x} = [u_{1x} + \alpha_{1x}(z,t)]\exp(iq_1 z), \quad (11a)$$

$$a_{1y} = [u_{1y} + \alpha_{1y}(z,t)]\exp(iq_2 z), \quad (11b)$$

$$a_{2x} = [u_{2x} + \alpha_{2x}(z,t)]\exp(iq_1 z), \quad (11c)$$

$$a_{2y} = [u_{2y} + \alpha_{2y}(z,t)]\exp(iq_2 z). \quad (11d)$$

Substituting Eq. (11) into Eq. (9) and linearizing, one can obtain

$$i\frac{\partial\alpha_{1x}}{\partial z}+i\frac{1}{v_{1x}}\frac{\partial\alpha_{1x}}{\partial t}+\kappa_{12x}\alpha_{2x}-\kappa_{12x}f_x\alpha_{1x}+R_{1x}[\alpha_{1x}+\alpha_{1x}^*]+Q_{1xy}[\alpha_{1y}+\alpha_{1y}^*]=0, \quad (12a)$$

$$i\frac{\partial\alpha_{1y}}{\partial z}+i\frac{1}{v_{1y}}\frac{\partial\alpha_{1y}}{\partial t}+\kappa_{12y}\alpha_{2y}-\kappa_{12x}f_y\alpha_{1y}+R_{1y}[\alpha_{1y}+\alpha_{1y}^*]+Q_{1xy}[\alpha_{1x}+\alpha_{1x}^*]=0, \quad (12b)$$

$$-i\frac{\partial\alpha_{2x}}{\partial z}+i\frac{1}{v_{2x}}\frac{\partial\alpha_{2x}}{\partial t}+\kappa_{21x}\alpha_{1x}-\kappa_{21x}f_x\alpha_{2x}+R_{2x}[\alpha_{2x}+\alpha_{2x}^*]+Q_{2xy}[\alpha_{2y}+\alpha_{2y}^*]=0, \quad (12c)$$

$$-i\frac{\partial\alpha_{2y}}{\partial z}+i\frac{1}{v_{2y}}\frac{\partial\alpha_{2y}}{\partial t}+\kappa_{21y}\alpha_{1y}-\kappa_{21x}f_y\alpha_{2y}+R_{2y}[\alpha_{2y}+\alpha_{2y}^*]+Q_{2xy}[\alpha_{2x}+\alpha_{2x}^*]=0, \quad (12d)$$

where $f_x=\frac{u_{2x}}{u_{1x}}$, $f_y=\frac{u_{2y}}{u_{1y}}$, $f_1=\frac{u_{1x}}{u_{1y}}$, $f_2=\frac{u_{2x}}{u_{2y}}$, the total power $p=u_{1x}^2+u_{2x}^2+u_{1y}^2+u_{2y}^2$, and

$$R_{1x}=\frac{p}{1+f_x^2+\left(\frac{1}{f_1}\right)^2+\left(\frac{f_x}{f_2}\right)^2}\gamma_{1x},$$

$$R_{1y}=\frac{p}{1+f_1^2+f_y^2+f_x^2f_1^2}\gamma_{1y},$$

$$R_{2x}=\frac{p}{1+\frac{1}{f_x^2}+\frac{1}{f_2^2}+\frac{1}{f_y^2f_2^2}}\gamma_{2x},$$

$$R_{2y}=\frac{p}{1+\left(\frac{f_1}{f_y}\right)^2+\frac{1}{f_y^2}+f_2^2}\gamma_{2x},$$

$$Q_{1xy}=\frac{p}{f_1\left[1+f_x^2+\left(\frac{1}{f_1}\right)^2+\left(\frac{f_x}{f_2}\right)^2\right]}\gamma_{1x}\,\rho,$$

$$Q_{2xy}=\frac{p}{f_2\left[1+\left(\frac{1}{f_2}\right)^2+\left(\frac{1}{f_x}\right)^2+\frac{1}{(f_2f_y)^2}\right]}\gamma_{2x}\,\rho.$$

To solve the above set of four linear differential equations, we assume a plane-wave ansatz of the form

$$\alpha_j(z,t)=c_j\exp[i(Kz-\Omega t)]+d_j\exp[-i(Kz-\Omega t)], \quad (13)$$

where K and Ω are the wave vector and frequency of perturbation. Substituting Eq. (13) in Eq. (12), we obtain a set of eight linearly coupled equations satisfied by c_j and d_j. This set has nontrivial solutions only when the 8×8 determinant formed by the coefficient matrix vanishes as given below:

$$\begin{pmatrix}\epsilon_{11}&\epsilon_{12}&\epsilon_{13}&\epsilon_{14}&\epsilon_{15}&\epsilon_{16}&\epsilon_{17}&\epsilon_{18}\\ \epsilon_{21}&\epsilon_{22}&\epsilon_{23}&\epsilon_{24}&\epsilon_{25}&\epsilon_{26}&\epsilon_{27}&\epsilon_{28}\\ \epsilon_{31}&\epsilon_{32}&\epsilon_{33}&\epsilon_{34}&\epsilon_{35}&\epsilon_{36}&\epsilon_{37}&\epsilon_{38}\\ \epsilon_{41}&\epsilon_{42}&\epsilon_{43}&\epsilon_{44}&\epsilon_{45}&\epsilon_{46}&\epsilon_{47}&\epsilon_{48}\\ \epsilon_{51}&\epsilon_{52}&\epsilon_{53}&\epsilon_{54}&\epsilon_{55}&\epsilon_{56}&\epsilon_{57}&\epsilon_{58}\\ \epsilon_{61}&\epsilon_{62}&\epsilon_{63}&\epsilon_{64}&\epsilon_{65}&\epsilon_{66}&\epsilon_{67}&\epsilon_{68}\\ \epsilon_{71}&\epsilon_{72}&\epsilon_{73}&\epsilon_{74}&\epsilon_{75}&\epsilon_{76}&\epsilon_{77}&\epsilon_{78}\\ \epsilon_{81}&\epsilon_{82}&\epsilon_{83}&\epsilon_{84}&\epsilon_{85}&\epsilon_{86}&\epsilon_{87}&\epsilon_{88}\end{pmatrix}\begin{pmatrix}c_1\\c_2\\c_3\\c_4\\d_1\\d_2\\d_3\\d_4\end{pmatrix}=0,$$

where $\epsilon_{11}=R_{1x}$, $\epsilon_{12}=0$, $\epsilon_{13}=Q_{1x}$, $\epsilon_{14}=0$, $\epsilon_{15}=R_{1x}+K-f_x\kappa_{12x}-\psi_{1x}$, $\epsilon_{16}=\kappa_{12x}$, $\epsilon_{17}=Q_{1x}$, $\epsilon_{18}=0$, $\epsilon_{21}=R_{1x}-K-f_x\kappa_{12x}+\psi_{1x}$, $\epsilon_{22}=\kappa_{12x}$, $\epsilon_{23}=Q_{1x}$, $\epsilon_{24}=0$, $\epsilon_{25}=R_{1x}$, $\epsilon_{26}=0$, $\epsilon_{27}=Q_{1x}$, $\epsilon_{18}=0$, $\epsilon_{31}=Q_{1x}$, $\epsilon_{32}=0$, $\epsilon_{33}=R_{1y}$, $\epsilon_{34}=0$, $\epsilon_{35}=Q_{1x}$, $\epsilon_{36}=0$, $\epsilon_{37}=R_{1y}+K-f_y\kappa_{12y}-\psi_{1y}$, $\epsilon_{38}=\kappa_{12y}$, $\epsilon_{41}=Q_{1x}$, $\epsilon_{42}=0$, $\epsilon_{43}=R_{1y}-K-f_y\kappa_{12y}+\psi_{1y}$, $\epsilon_{44}=\kappa_{12y}$, $\epsilon_{45}=Q_{1x}$, $\epsilon_{46}=0$, $\epsilon_{47}=R_{1y}$, $\epsilon_{48}=0$, $\epsilon_{51}=0$, $\epsilon_{52}=R_{2x}$, $\epsilon_{53}=0$, $\epsilon_{54}=Q_{2x}$, $\epsilon_{55}=\kappa_{12x}$, $\epsilon_{56}=R_{2x}-K-\frac{\kappa_{12x}}{f_x}-\psi_{2x}$, $\epsilon_{57}=0$, $\epsilon_{58}=Q_{2x}$, $\epsilon_{61}=\kappa_{21x}$, $\epsilon_{62}=R_{2x}+K-\frac{\kappa_{12x}}{f_x}+\psi_{2x}$, $\epsilon_{63}=0$, $\epsilon_{64}=Q_{2x}$, $\epsilon_{65}=0$, $\epsilon_{66}=R_{2x}$, $\epsilon_{67}=0$, $\epsilon_{68}=Q_{2x}$, $\epsilon_{71}=0$, $\epsilon_{72}=Q_{2x}$, $\epsilon_{73}=0$, $\epsilon_{74}=R_{2y}$, $\epsilon_{75}=0$, $\epsilon_{76}=Q_{2x}$, $\epsilon_{77}=\kappa_{21y}$, $\epsilon_{78}=R_{2y}-K-\frac{\kappa_{21y}}{f_y}-\psi_{2y}$, $\epsilon_{81}=0$, $\epsilon_{82}=Q_{2x}$, $\epsilon_{83}=\kappa_{21y}$, $\epsilon_{84}=R_{2y}+K-\frac{\kappa_{21y}}{f_y}+\psi_{2y}$, $\epsilon_{85}=0$, $\epsilon_{86}=Q_{2x}$, $\epsilon_{87}=0$, $\epsilon_{88}=R_{2y}$, and $\psi_{ij}=\frac{\Omega}{v_{igj}}$ ($i=1,2$ and $j=x,y$).

In the general case, $v_{1gx}\neq v_{2gx}\neq v_{1gy}\neq v_{2gy}$; but in this paper in order to highlight the most important physical effects in the ODC, we assume $v_{1gx}=v_{2gx}=v_{1gy}=v_{2gy}$; $\gamma_{1x}=\gamma_{1y}=\gamma_1$ and $\gamma_{2x}=\gamma_{2y}=\gamma_2$; $f_x=f_y=f$. The vanishing condition of the determinant associated with this 8×8 stability matrix leads to an eighth-order polynomial in ψ as given below:

$$\psi^8+a_6\psi^6+a_5\psi^5+a_4\psi^4+a_3\psi^3+a_2\psi^2+a_1\psi+a_0=0. \quad (14)$$

The eight roots of Eq. (14) determine the stability of the continuous-wave solution. To observe MI, one of the roots of this eighth-order polynomial should possess a nonzero and negative imaginary part. The expression for the instability gain is given by the equation

$$g=|\mathrm{Im}(\psi_{\max})|, \quad (15)$$

where $\mathrm{Im}(\psi_{\max})$ denotes the imaginary part of $\psi_{\max}$, $\psi_{\max}$ is the root of the polynomial with the largest value.

III. MODULATION INSTABILITY IN BIREFRINGENT OPPOSITELY DIRECTED COUPLER

The propagation of electromagnetic waves with two polarized modes in ODC possesses birefringence. According to the polarized modes supported by the wave guide, the birefringence may be linear or circular. In the case of linear birefringence, the core is said to support two orthogonal linearly polarized modes. On other hand, the circular-birefringent ODC supports the right- and left-circularly polarized modes. For better insight, we consider both types of birefringence, namely, linear and circular birefringence. To provide a comprehensive picture, we study MI in both normal and anomalous dispersion regimes.

A. Normal dispersion

In this section, we briefly study MI in a normal dispersion regime, where $\mathrm{sgn}(f)=1$. It is well known that, due to the lack of phase matching between the linear and nonlinear effects, a normal dispersion regime is not subjected to MI. However, under some special cases such as in the presence of higher order dispersion or cross-phase modulation [40–42], noninstantaneous nonlinear systems [43], directional couplers [1], MI was observed even in the normal dispersion regime. To

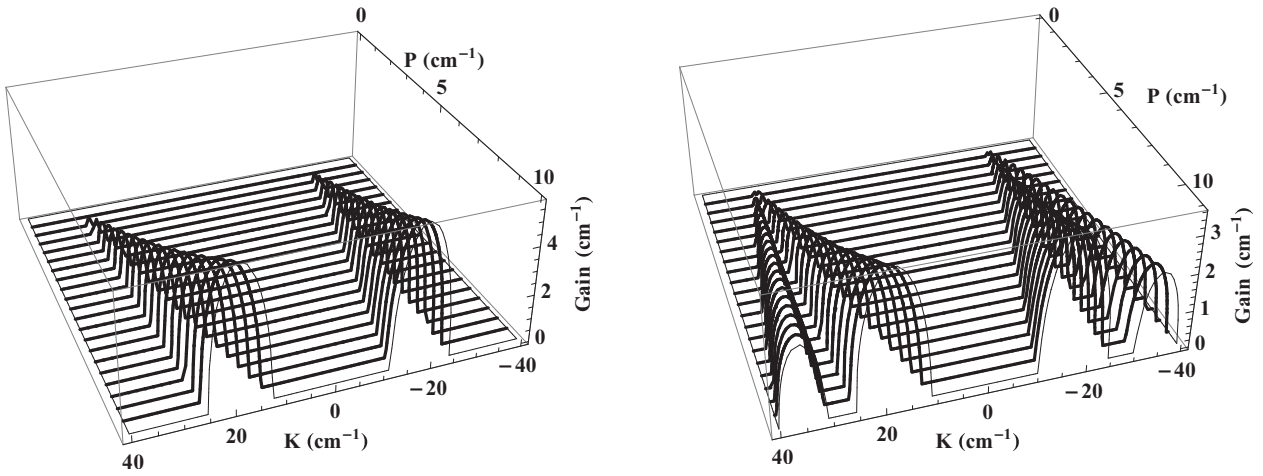

FIG. 2. MI gain spectra vs power P in the normal dispersion regime in a linear-birefringent ODC for different nonlinear configurations: (a) $\gamma_1 = \gamma_2 = 1$ and (b) $\gamma_1 = -\gamma_2 = 1$.

report on the influence of birefringence on the MI spectra of ODCs, we consider the two typical birefringence cases, linear and circular, whose cross-phase modulation coefficients take the values $\sigma = 2/3$ and $\sigma = 2$, respectively.

1. Effect of input power on MI

Now we discuss the effect of the input wave power P on the instability spectra of birefringent ODCs. As reported earlier [1,25], the instability gain is found to increase monotonously with increase in the input power [1]. Figure 2 depicts the MI gain spectra versus power P for different nonlinear configurations in linear-birefringent ODC. Two nonlinear combinations will be considered in this context, i.e., $\gamma_1 = \gamma_2 = 1$ and $\gamma_1 = -\gamma_2 = 1$. When $\gamma_1 = \gamma_2 = 1$, the instability spectra consist of symmetric instability bands centered at zero perturbation constant as shown in the Fig. 2(a). As the input power increases, the instability gain and the width of the instability band proportionally increase. But the scenario is different for the defocusing nonlinear configuration. For instance, when $\gamma_1 = -\gamma_2 = 1$, new symmetric instability bands at higher values of K are noted, in addition to the primary pair of instability bands. Thus, the defocusing nonlinearity enables new instability bands and thereby extends the domain of the instability region as shown in Fig. 2(b).

Figure 3 represents the MI spectra corresponding to circular birefringence for the nonlinear configurations $\gamma_1 = \gamma_2 = 1$ and $\gamma_1 = -\gamma_2 = 1$. It is evident from Fig. 3(a) for $\gamma_1 = \gamma_2 = 1$, in addition to the symmetric central band as observed for the linear-birefringent case, a symmetric band of less gain and narrow width is observed for the circular-birefringent system. On the other hand, the defocusing nonlinear configuration $\gamma_1 = -\gamma_2 = 1$ enhances MI by increasing gain and width of the instability band.

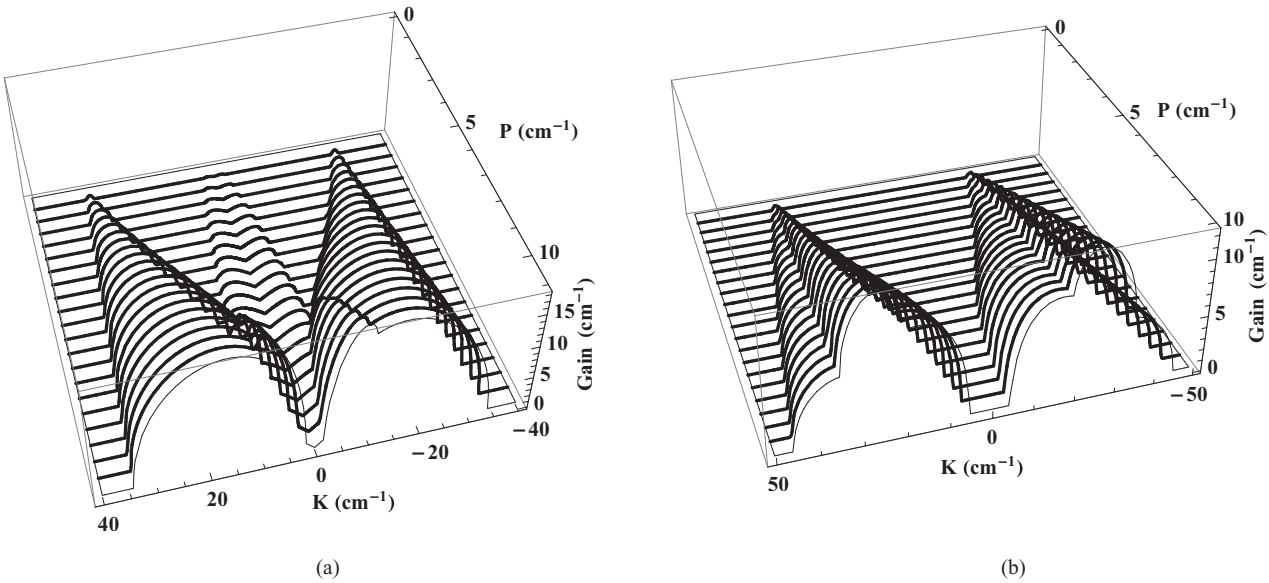

FIG. 3. Same as Fig. 2, but in a circular-birefringent ODC.

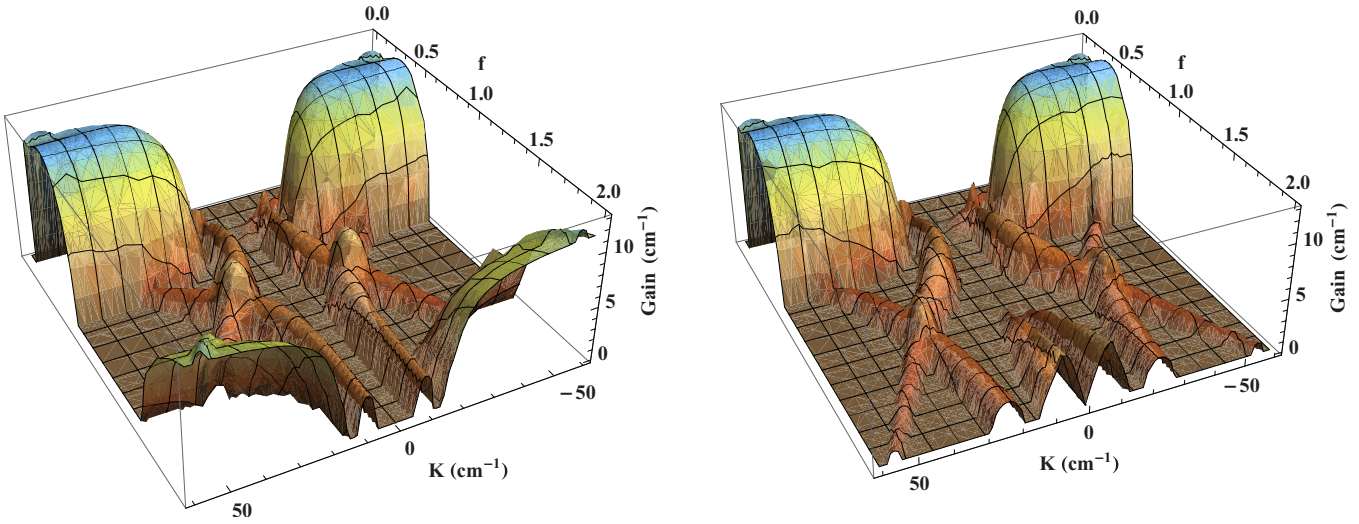

FIG. 4. MI gain spectra vs f in the normal dispersion regime in a linear-birefringent ODC for different nonlinear configurations: (a) $\gamma_1 = \gamma_2 = 1$ and (b) $\gamma_1 = -\gamma_2 = 1$.

2. *Effect of the wave amplitude ratio on MI*

Xiang *et al.* investigated MI in ODCs without considering birefringent effects such as cross-phase modulation and polarization-dependent coupling between the cores [22]. It is reported that in ODCs, the nonlinear PIM channels form symmetric MI bands at lower f values and nonlinear NIM channels form MI bands at higher values of f [25]. In similar lines with [22,25], one can observe two pairs of instability bands on either side of K, the one corresponding to lower values of f represents the PIM band and the other at higher values of f corresponds to the NIM band. Figure 4 shows the MI gain spectra versus f for different nonlinear configurations in linear-birefringent ODCs.

Besides the PIM and NIM bands, one can observe new symmetric instability bands in Fig. 4, which ares identified as the result of the birefringence and we call them birefringent bands. The birefringent bands are generally weak, which is reflected by the less gain and narrow width of the instability bands. In similar lines with inherent PIM and NIM bands in the ODC, the emergence of two pairs of birefringent bands is identified as the result of the nonlinear PIM and NIM channels. It is worth mentioning that the two pairs of birefringent bands are reduced to one pair if either PIM ($\gamma_1 = 0$) or NIM ($\gamma_2 = 0$) is turned off. This is a clear indication that the inclusion of birefringence induces new bands in addition to the intrinsic PIM and NIM bands. The birefringent band identified at the lower values of f is called the birefringent PIM band (B-PIM) and the one at the higher values of f is called the birefringent NIM band (B-NIM). As evident in Fig. 4(a), the two birefringent bands overlap at a particular value of f, which is marked by an abrupt increase in the MI gain.

Figure 4(b) depicts the instability spectra corresponding to defocusing nonlinearity, i.e., $\gamma_1 = -\gamma_2 = 1$. It is obvious from the Fig. 4(b) that the defocusing nonlinearity does not bring any new instability band, instead it suppresses the NIM band, causing depletion in the gain and width of the instability band. However, the birefringent bands show no significant changes caused by the defocusing nonlinearity.

Following the linear-birefringent case, we now extend our study to the case of circular-birefringent ODCs. Figure 5 depicts the MI gain spectra versus f in the normal dispersion regime for nonlinear configurations $\gamma_1 = \gamma_2 = 1$ and $\gamma_1 = -\gamma_2 = 1$. As reported in the linear birefringence, the PIM and NIM bands remain independent of birefringence even for the circular case.

Its worth mentioning that the two birefringent bands (B-PIM and B-NIM) as a result of circular birefringence dominate the inherent PIM and NIM bands of the ODC. This preponderance is attributed to the fact that the cross-phase modulation effect for circular birefringence is stronger, thus allowing a better coupling between the beams, which results in the enhancement of the gain. It is interesting to note that for $f \approx 1$, the B-PIM and B-NIM bands merge, resulting in the coalesced instability region of elevated gain as shown in Fig. 5. Figure 5(b) corresponds to the case of defocusing nonlinearity in the circular-birefringent system. It is evident from Fig. 5(b), that there is no significant impact on the birefringent bands; however, defocusing nonlinearity suppresses the NIM band by depleting the gain and width of the instability region.

B. Anomalous dispersion

Now, we extend our study to the case of anomalous dispersion regime, where $\mathrm{sgn}(f) = -1$. It is well known that the anomalous dispersion regime is said to support the formation of solitons and MI as a result of the interplay between the nonlinearity and the negative group dispersion coefficient. Thus, the study of MI in the anomalous dispersion regime deserves special interest. In this section, we briefly study the impact of birefringence on MI in the context of anomalous dispersion regime.

As discussed in the previous section, we consider both kinds of birefringence, namely, linear and circular. In similar lines to

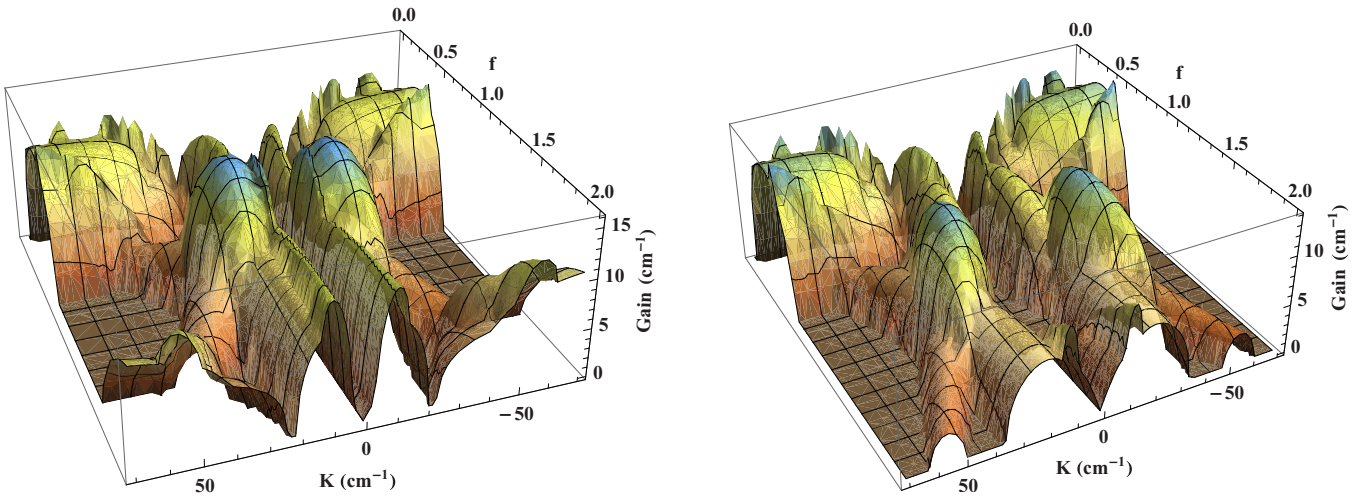

FIG. 5. Same as Fig. 4, but in a circular-birefringent ODC.

the case of normal dispersion regime, in the following sections, we exclusively study the impact of input power P and the wave amplitude ratio f on the instability spectra of birefringent ODC.

1. Effect of input power on MI

The dependence of power on MI for different nonlinear configurations in the anomalous dispersion regime is shown in Fig. 6, which clearly illustrates the monotonous increase in the MI gain with input power. In the linear-birefringent case, two pairs of symmetric instability bands on either side of the zero propagation constant for $\gamma_1 = \gamma_2 = 1$ are observed as shown in the Fig. 6(a). This is in contrast to the single pair of instability bands noted for the case of the normal dispersion regime (refer to Fig. 2). The primary band near the zero propagation constant shows higher gain than the instability band at higher values of K. Figure 6(b) shows the instability spectra when the nonlinearity of the NIM channel is defocused. It is observed that for defocusing nonlinearity, the primary band near the zero propagation constant shifts to higher values of K, and resembles the MI spectra corresponding to the case of the normal dispersion regime (refer to Fig. 2).

The instability spectra corresponding to the circular-birefringent case is portrayed in the Fig. 7. As for linear birefringence, two pairs of instability bands are observed on either side of the zero propagation constant. It is interesting to note that the gain of the instability band is found to be significantly larger than in the linear-birefringent case as shown in Fig. 7(a). Figure 7(b) depicts the instability band when the nonlinearity is defocused. It is observed that the instability bands shift toward the higher values of K for defocusing nonlinearity; interestingly, one can see that the gain of the instability band is greater by a significant factor than its linear counterpart [refer to Fig. 6(b)].

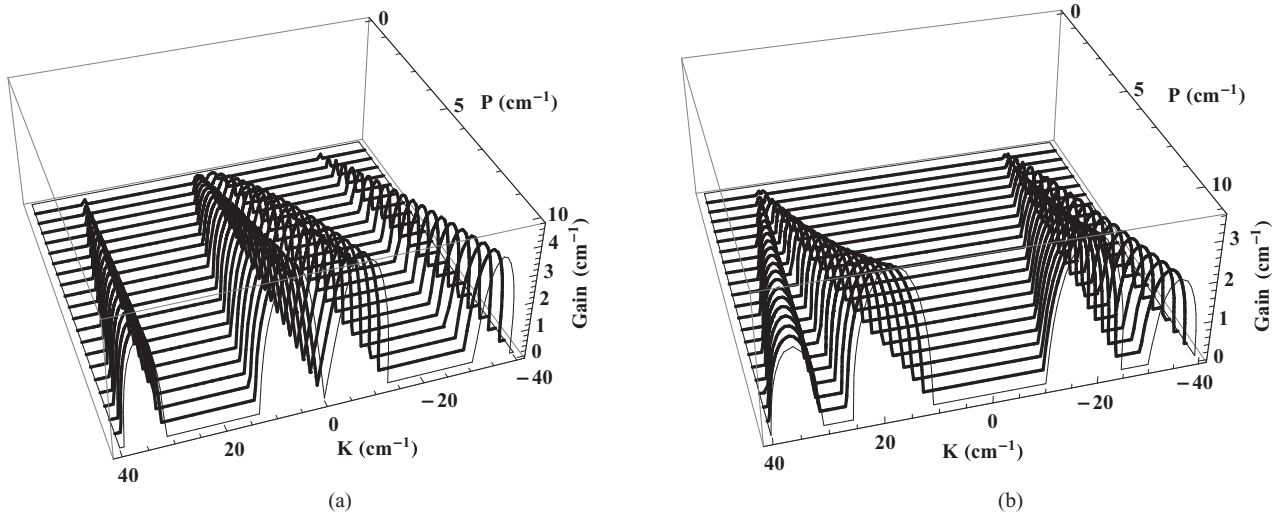

FIG. 6. MI gain spectra vs power P in the anomalous dispersion regime in a linear-birefringent ODC for different nonlinear configurations: (a) $\gamma_1 = \gamma_2 = 1$ and (b) $\gamma_1 = -\gamma_2 = 1$.

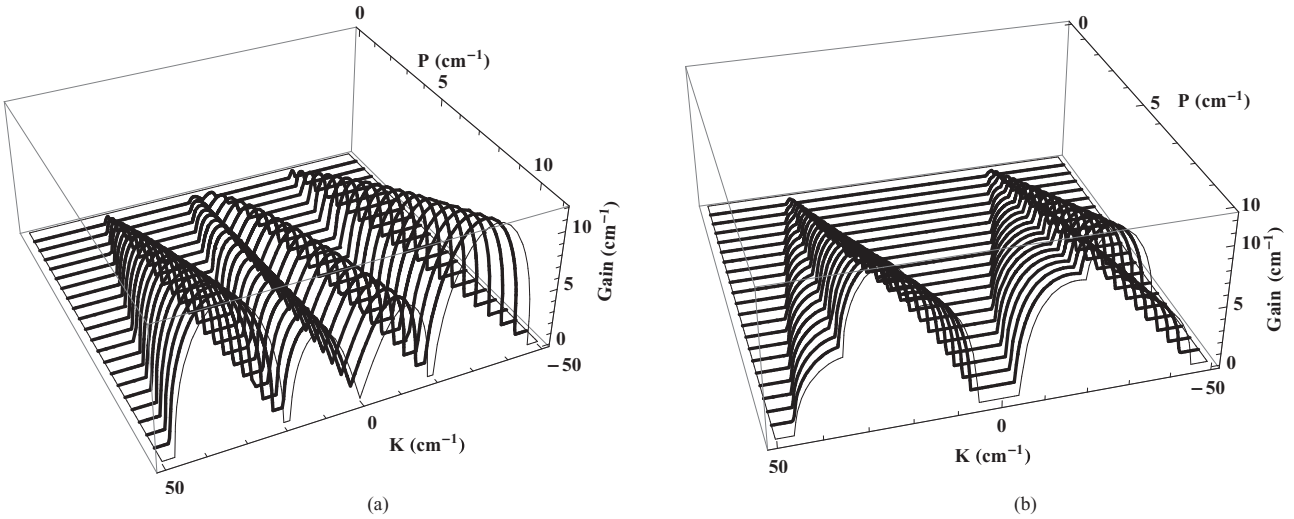

FIG. 7. Same as Fig. 6, but in a circular-birefringent ODC.

2. *Effect of wave amplitude ratio on MI*

The influence of the input wave amplitude ratio f on MI corresponding to the linear-birefringent case is depicted in Fig. 8. As in the case of a normal dispersion regime, one can notice two pairs of instability bands, which are identified as a characteristic feature of ODCs. In addition to the PIM-NIM band, the impact of birefringence results in the emergence of an additional two pairs of birefringent bands (B-PIM and B-NIM). The B-PIM arises at the lower values of f and the B-NIM is typically observed at the higher values of f. The B-PIM and B-NIM bands collide at a particular value of f, which results in the abrupt increase in the MI gain as evident from Fig. 8(a). Figure 8(b) represents the instability spectra as a function of f for defocusing nonlinearity. The defocusing nonlinearity is found to enhance the instability band corresponding to the NIM channel, which is evident from the increase in gain and width of the NIM band. However the PIM band and the birefringent band hardly show any changes in the MI gain.

Figure 9 depicts the instability spectra corresponding to the circular-birefringent ODC as a function of f. One can clearly see the dramatic increase in the gain of the birefringent band in comparison to the linear-birefringent counterpart. The dramatic increase in the gain of the birefringent band in the circular case is a consequence of the enhanced coupling between the beams due to higher values of the cross-phase coupling coefficient. The B-PIM and B-NIM bands dominate the inherent PIM and NIM bands in terms of the gain, and a hump with higher gain is noticed at a particular value of f. The number of instability bands remains constant, and the type of birefringence (linear or circular) is found to effect only the gain and width of the instability bands. The instability spectra corresponding to the defocusing nonlinearity are shown in the Fig. 9(b); as in the case of linear birefringence, the defocusing

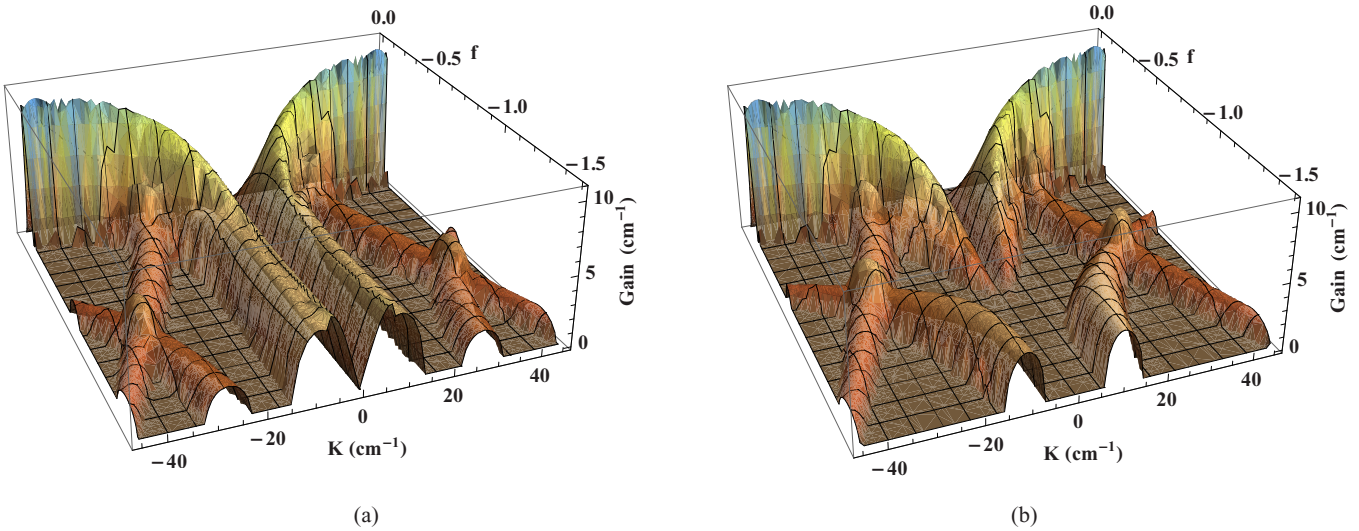

FIG. 8. MI gain spectra vs f in the anomalous dispersion regime in a linear-birefringent ODC for different nonlinear configurations: (a) $\gamma_1 = \gamma_2 = 1$ and (b) $\gamma_1 = -\gamma_2 = 1$.

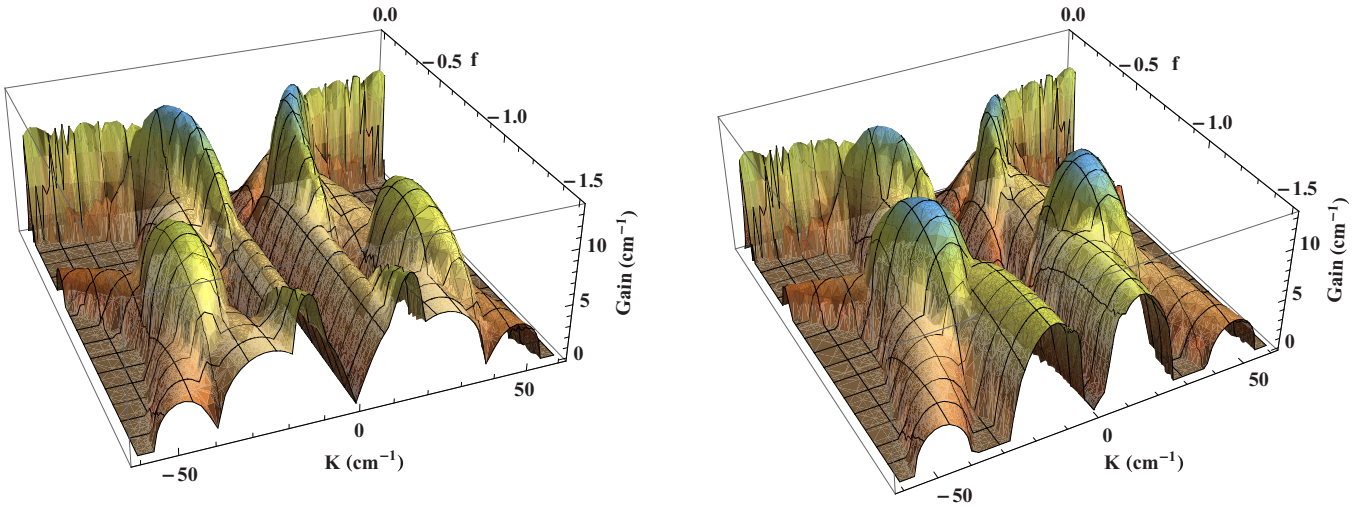

FIG. 9. Same as Fig. 8, but in a circular-birefringent ODC.

nonlinearity enhances the instability band corresponding to NIM channel. However, a significant increase in the gain of the NIM band of circular birefringence is evident in Fig. 9(b), in comparison to the linear counterpart shown in Fig. 8(b).

IV. SUMMARY AND CONCLUSION

We have investigated MI in linear- and circular-birefringent ODCs with NIM channels. We extended our study in both normal and anomalous dispersion regimes for different nonlinear configurations of the coupler channel. Special attention was given to investigating the effect of input power and wave amplitude ratio f on the instability spectra. It is found that besides the nonlinear PIM and NIM bands, one can observe new instability bands, which are identified as resulting from the birefringence, as shown in Table I. It is also noted that the birefringent bands (B-PIM and N-PIM) are characteristic of the nonlinear PIM and NIM channels. It is observed that the defocusing nonlinearity suppresses the NIM band in the normal dispersion regime, whereas in anomalous dispersion regimes, the defocusing nonlinearity enhances the gain of the NIM band.

In contrast to the case of linear birefringence, in terms of MI gain only two birefringent bands dominate when considering circular birefringence: the inherently PIM and NIM bands. This preponderance is attributed to the fact that the cross-phase modulation effect for circular birefringence is stronger, thus allowing a better coupling between the beams, which results in the enhancement of the gain. Therefore, the manipulation of MI and solitons in oppositely directed couplers is better performed when the birefringence is circular rather than linear. Thus we report ways to generate and manipulate MI and solitons in birefringent ODCs with a particular emphasis on a NIM channel. These theoretical results could provide some guidelines in the design and development of ODC-based devices.

ACKNOWLEDGMENTS

K.P. thanks DST, CSIR, NBHM, IFCPAR, and DST- FCT, Government of India, for financial support through major projects. A.K.S.A. thanks DST for financial support through THE PURSE scheme. K.N. thanks CSIR, for providing SRF financial support. The research of A.I.M. was supported by the Russian Science Foundation (Project No. 14-22-00098).

TABLE I. Summary of MI in birefringent oppositely directed couplers.

	NL configuration		NIM	PIM	B-NIM	B-PIM
Birefringence	γ_1	γ_2	band	band	band	band
	1	0		✓		✓
	0	1	✓		✓	
Linear	1	1	✓	✓	✓	✓
	1	−1	✓	✓	✓	✓
	1	0		✓		✓
	0	1	✓		✓	
Circular	1	1	✓	✓	✓	✓
	1	−1	✓	✓	✓	✓

[1] G. P. Agrawal, *Nonlinear Fiber Optics*, 5th Ed. (Academic, San Diego, 2013).
[2] M. J. Potasek, Opt. Lett. **12**, 921 (1987).
[3] P. K. Shukla and J. J. Rasmussen, Opt. Lett. **11**, 171 (1986).
[4] K. Porsezian, K. Nithyanandan, R. Vasantha Jayakantha Raja, and P. K. Shukla, J. Opt. Soc. Am. B **29**, 2803 (2012).
[5] P. V. Mamyshev, C. Bosshard, and G. I. Stegeman, J. Opt. Soc. Am. B **11**, 1254 (1994).
[6] A. Hasegawa, Opt. Lett. **9**, 288 (1984).
[7] K. Tai, A. Hasegawa, and A. Tomita, Phys. Rev. Lett. **56**, 135 (1986).
[8] T. B. Benjamin and J. E. Feir, J. Fluid Mech. **27**, 417 (1967).
[9] G. A. Askar'yan, Sov. Phys. JETP **15**, 1088 (1962).
[10] T. Taniuti and H. Washimi, Phys. Rev. Lett. **21**, 209 (1968).
[11] A. Hasewaga, Phys. Rev. Lett. **24**, 1165 (1970).
[12] V. I. Bespalov and V. I. Talanov, Pis'ma Zh. Eksp. Teor. Fiz. **3**, 471 (1966).
[13] L. A. Ostrovskii, Sov. Phys. JETP, **24**, 797 (1967).
[14] K. Nithyanandan, R. Vasantha Jayakantha Raja, K. Porsezian, and B. Kalithasan, Phys. Rev. A **86**, 023827 (2012).
[15] D. Anderson and M. Lisak, Opt. Lett. **9**, 468 (1984).
[16] S. B. Cavalcanti, J. C. Cressoni, H. R. da Cruz, and A. S. Gouveia-Neto, Phys. Rev. A **43**, 6162 (1991).
[17] K. Nithyanandan, R. Vasantha Jayakantha Raja, and K. Porsezian, J. Opt. Soc. Am. B **30**, 178 (2013).
[18] N. M. Litchinitser, I. R. Gabitov, and A. I. Maimistov, Phys. Rev. Lett. **99**, 113902 (2007).
[19] V. E. Kazantseva, A. I. Maimistov, and S. S. Ozhenko, Phys. Rev. A **80**, 043833 (2009).
[20] A. K. Shafeeque Ali, K. Porsezian, and T. Uthayakumar, Phys. Rev. E **90**, 042910 (2014).
[21] A. Alu and N. Engheta, in *Negative Refraction Metamaterials*, edited by G. V. Eleftheriades and K. G. Balmain (Wiley, New York, 2005).
[22] Yuanjiang Xiang, Shuangchun Wen, Xiaoyu Dai, and Diayuan Fan, Phys. Rev. E **82**, 056605 (2010).
[23] P. H. Tatsing, A. Mohamadou, C. Bouri, C. G. Latchio Tiofack, and T. C. Kofane, J. Opt. Soc. Am. B **29**, 3218 (2012).
[24] A. Mohamadouabc, P. H. Tatsing, C. G. Latchio Tiofack, C. B. Tabi, and T. C. Kofane, J. Mod. Opt. **61**, 1670 (2014).
[25] A. K. Shafeeque Ali, K. Nithyanandan, and K. Porsezian, Phys. Lett. A **379**, 223 (2015).
[26] Jinggui Zhang, Xiaoyu Dai, Lifu Zhang, Yuanjiang Xiang, and Yongfan Li, J. Opt. Soc. Am. B **32**, 1 (2015).
[27] N. Akhmediev and J. M. Soto-Crespo, Phys. Rev. E **49**, 5742 (1994).
[28] B. A. Malomed, Phys. Rev. A **43**, 410 (1991).
[29] B. Kalithasan, K. Nakkeeran, K. Porsezian, P. Tchofo Dinda, and N. Mariyappa, J. Opt. A: Pure Appl. Opt. **10**, 085102 (2008).
[30] G. Millot, P. Tchofo Dinda, E. Seve, and S. Wabnitz, Opt. Fiber Technol. **7**, 170 (2001).
[31] S. Wabnitz, Phys. Rev. A **38**, 2018 (1988).
[32] J. E. Rothenberg, Phys. Rev. A **42**, 682 (1990).
[33] H. S. Chiu and K. W. Chow, Phys. Rev. A, **79**, 065803 (2009).
[34] M Nakazawa, H. Kubota, K Suzuki, and E. Yamada, Chaos **10**, 486 (2000).
[35] B. Frisquet, B. Kibler, J. Fatome, P. Morin, F. Baronio, M. Conforti, G. Millot, and S. Wabnitz, Phys. Rev. A **92**, 053854 (2015).
[36] F. Baronio, M. Conforti, A. Degasperis, S. Lombardo, M. Onorato, and S. Wabnitz, Phys. Rev. Lett. **113**, 034101 (2014).
[37] F. Baronio, S. Chen, P. Grelu, S. Wabnitz, and M. Conforti, Phys. Rev. A **91**, 033804 (2015).
[38] A. D. Boardman and G. S. Cooper, J. Opt. Soc. Am. B. **5**, 403 (1988).
[39] A. D. Boardman and G. S. Cooper, J. Mod. Opt. **35**, 407 (1988).
[40] J. H. Li, K. S. Chiang, B. A. Malomed, and K. W. Chow, J. Phys. B: At. Mol. Opt. Phys. **45**, 165404 (2012).
[41] J. D. Harvey, R. Leonhardt, S. Coen, G. K. L. Wong, J. C. Knight, W. J. Wadsworth, and P. St. J. Russell, Opt. Lett. **28**, 2225 (2003).
[42] K. Nithyanandan and K. Porsezian, Opt. Commun. **303**, 46 (2013).
[43] G. L. da Silva, I. Gleria, M. L. Lyra, and A. S. B. Sombra, J. Opt. Soc. Am. B **26**, 183 (2009).